

ROVR-Open-Dataset: A Large-Scale Depth Dataset for Autonomous Driving

Xianda Guo^{1,*}, Ruijun Zhang^{2,*}, Yiqun Duan^{3,*}, Ruilin Wang², Keyuan Zhou⁴, Wenzhao Zheng⁵,
Wenke Huang¹, Gangwei Xu⁸, Mike Horton⁶, Yuan Si⁶, Hao Zhao^{7,4,†}, Long Chen^{2,†}

¹ School of Computer Science, Wuhan University ² CASIA ³ University of Technology Sydney

⁴ Zhejiang University ⁵ University of California, Berkeley ⁶ ROVR Labs, Inc.

⁷ AIR, Tsinghua University ⁸ Huazhong University of Science and Technology

xianda_guo@163.com; yuan.si@rovr.network

Abstract—Depth estimation is a fundamental task for 3D scene understanding in autonomous driving, robotics, and augmented reality. Existing depth datasets, such as KITTI, nuScenes, and DDAD, have advanced the field but suffer from limitations in diversity and scalability. As benchmark performance on these datasets approaches saturation, there is an increasing need for a new generation of large-scale, diverse, and cost-efficient datasets to support the era of foundation models and multi-modal learning. To address these challenges, we introduce a large-scale, diverse, frame-wise continuous dataset for depth estimation in dynamic outdoor driving environments, comprising 20K video frames to evaluate existing methods. Our lightweight acquisition pipeline ensures broad scene coverage at low cost, while sparse yet statistically sufficient ground truth enables robust training. Compared to existing datasets, ours presents greater diversity in driving scenarios and lower depth density, creating new challenges for generalization. Benchmark experiments with standard monocular depth estimation models validate the dataset’s utility and highlight substantial performance gaps in challenging conditions, establishing a new platform for advancing depth estimation research. Dataset will be available at <https://xiandaguo.net/ROVR-Open-Dataset/>

I. INTRODUCTION

Depth estimation [1], [2] is a cornerstone of 3D scene understanding, providing essential geometric information for a wide range of applications, including autonomous driving [1], [2], [3], robotics [4], and augmented reality (AR) [5]. Accurate depth maps enable downstream tasks such as obstacle detection, motion planning, semantic mapping, and human-machine interaction. Over the past decade, the availability of high-quality annotated datasets has been a major driver of progress in this field, enabling the development of increasingly sophisticated learning-based approaches. Notable examples include large-scale driving datasets such as KITTI [6], [7], nuScenes [8], and DDAD [9], which have served as critical benchmarks for monocular and stereo depth estimation. However, despite their impact, each of these datasets presents limitations in one or more aspects, including scene diversity, annotation density, sensor calibration, and scalability. KITTI [10], while offering high-precision LiDAR depth, is restricted to a relatively narrow set of urban and suburban scenarios, and its limited scale constrains the training of high-capacity models. nuScenes [8] broadens the range of environments and weather conditions but suffers from lower-quality ground truth due to LiDAR calibration

inaccuracies. DDAD [9] achieves dense and long-range depth measurements using a sophisticated multi-sensor setup, yet its reliance on costly hardware and complex calibration makes large-scale collection economically challenging.

With the rapid evolution of deep neural networks—particularly transformer-based architectures [1], [11], [12] and multi-modal foundation models—there has been a significant surge in demand for large-scale, diverse, and challenging datasets. As the capacity of models grows, their performance on existing benchmarks is approaching saturation, leaving diminishing room for further improvement without fundamentally new data sources. This trend is especially evident in autonomous driving, where domain-specific datasets can no longer keep pace with the generalization requirements of modern models.

Meanwhile, as long as the model capacity increases, the benchmark performance of emerging models based on these datasets is approaching the limitation in the near future. Facing the new era of foundation models and multi-modal LLMs, we aimed to first propose a very large-scale 3D depth dataset series in diverse driving scenarios, and continuously scale up to other spatial understanding challenges for multi-modal foundation models.

We present a new *large-scale, diverse, frame-wise continuous, and cost-efficient* public dataset for depth estimation in dynamic outdoor environments as the first version of the dataset with 200K video frames, and will scale up to 1 million very soon. Our collection spans a wide variety of scenes and conditions while maintaining low capture cost through a lightweight acquisition pipeline. Compared to existing datasets, our ground-truth depth is *sparse* but statistically sufficient for training robust depth estimators. The dataset is fully extensible, enabling future scaling in both volume and scene diversity with minimal additional cost.

Beyond providing large-scale training data, our dataset introduces *new challenges* for the community: the driving diversity is significantly higher and differs from those in KITTI or DDAD, requiring models to adapt to varying sampling distributions, demanding stronger generalization ability; meanwhile, the depth GT density is lower than existing benchmarks, which is harder for model to learn. We summarize key comparison against existing datasets in Table I, present scene-wise distributions in Table II, and show representative samples in Figure 2. The capture setup and sensor configuration are illustrated in Figure 1. We further

*These authors contributed equally to this work.

†Corresponding authors

TABLE I: Comparison of available autonomous driving depth datasets.

Dataset	Scenario	Frames		Resolution	Labels
KITTI _{Depth} [10]	Driving	85k	7k	1226 × 370	✓
nuScenes [8]	Driving	34149	5851	1600 × 900	✓
DDAD [9]	Driving	17,050	4,150	1936 × 1216	✓
ROVR (Ours)	Driving	193,648	10,002	1920 × 1280	✓

benchmark standard monocular depth estimation baselines on our dataset (Section IV), demonstrating its utility and the remaining gap to close in challenging scenarios. To provide a technical understanding of the proposed ROVR open dataset, we benchmarked several top-ranked KITTI models in Table IV and domain-specific testing in Table V. Notably, KITTI SOTA models are far from saturating depth estimation metrics on ROVR, highlighting its greater difficulty and broader coverage of real-world scenarios. ROVR provides a crucial platform for developing depth estimation models with stronger generalization to complex, dynamic, real-world scenarios.

II. RELATED WORK

Autonomous Driving Depth Datasets. The *KITTI* benchmark [6] is one of the earliest and most widely used datasets for driving-scene depth estimation, providing stereo imagery and sparse LiDAR ground truth up to ~ 80 m (85K/7K, 1226×370). It mainly covers urban and highway scenes under fair weather, limiting diversity in environmental conditions and viewpoints. *nuScenes* [8] extends to a 360° multi-camera setup with 32-beam LiDAR, radar, and GPS/IMU, collected in Boston and Singapore (34K/5.8K, 1600×900). It offers broader variety—including night and rain—but yields sparser per-image depth due to lower-resolution LiDAR. *DDAD* [9] addresses range and density constraints via long-range (250 m) high-density LiDAR and high-resolution cameras, providing near-dense depth for diverse urban scenes across multiple continents (17K/4.1K, 1936×1216).

Other Depth Datasets. A variety of datasets target depth estimation beyond autonomous driving scenarios, covering indoor, outdoor, and mixed environments, as well as synthetic domains. *NYUv2* [13] provides 795 training and 654 test frames at 640×480 resolution for indoor RGB-D scenes. *ScanNet* [14] offers a large-scale collection of 2.5M frames with dense annotations for mixed indoor environments at the same resolution. *MegaDepth* [15] supplies ~ 128 K internet-photo-derived frames via multi-view stereo, spanning diverse indoor/outdoor scenes. *TUM RGB-D* [16] focuses on benchmarking depth and camera pose estimation with 640×480 resolution RGB-D sequences. Synthetic datasets such as *SceneNet RGB-D* [17] (5M training and 300K test frames, 320×240) enable controlled, noise-free depth generation for pre-training and domain adaptation. Driving-oriented datasets like *Cityscapes* [18], *RobotCar* [19], and *KITTI_{Depth}* [10] expand coverage for outdoor urban scenes, with *KITTI_{Depth}* offering 85K/7K stereo frames with ground-truth depth. More recent large-scale driving datasets include *Driving-*

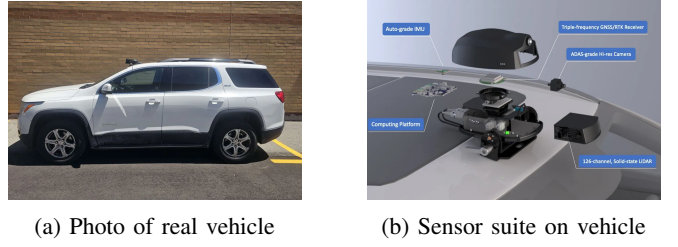


Fig. 1: Illustration of the data collection vehicles: (a) real-world vehicle used for urban field tests; (c) sensor suite on Vehicle 3 including IMU, GNSS/RTK, camera, LiDAR, and computing platform.

Stereo [20] (174K/7.7K frames, 1762×800), *nuScenes* [8] (34K/5.8K frames, 1600×900), *DDAD* [9] (17K/4.1K frames, 1936×1216), and *Waymo* [21] (600K frames, 1920×1280). Mixed-scene datasets such as *DIODE* [22] and *DA-2K* [11] offer diverse environments with dense depth, while our proposed *ROVR* dataset provides 193K/10K high-resolution (1920×1280) driving frames with centimeter-level accuracy.

Monocular Depth Estimation. The introduction of end-to-end trainable neural networks in MMDE, pioneered by [23], marked a milestone by introducing optimization with the scale-invariant log loss (SI_{log}). Subsequent advances span convolution-based architectures [24], [25], [26], [27], diffusion-based models [2] and transformer-based models [28], [29], [30], [31], [1], achieving impressive in-domain accuracy—e.g., PackNet [9], DPT [32], and AdaBins [29] report 5–6% relative error on KITTI, approaching LiDAR precision. However, these models often overfit to their training domain and degrade sharply in novel scenes. To improve cross-domain generalization, recent works explore large-scale and diverse training data, as in the *Depth-Anything* series [12], [33], or adopt generalizable MMDE strategies [34], [35], [36] that incorporate camera awareness [37], [35] or normalize outputs via intrinsics [38], [39], [36]. While geometric pretraining [34] and dataset-specific priors [36] can boost zero-shot accuracy, these methods typically assume noiseless pinhole intrinsics and rely on predefined backprojection, limiting applicability. Benchmarks such as the Monocular Depth Estimation Challenge (MDEC) now track both in-domain and zero-shot performance, with *DepthAnything v2* and *Marigold* [40] as strong recent baselines.

III. ROVR DATASETS

In this section, we introduce the ROVR OpenDataset, a large-scale open 3D dataset tailored for autonomous driving, robotics, and 4D perception tasks. We first describe the data acquisition system, where synchronized LiDAR point clouds and high-resolution images are collected. We then outline the sensor configuration and data collection protocol.

A. Data Acquisition

The dataset was collected using multiple ROVR data collection vehicles deployed across **North America, Europe, and Asia**. Each vehicle is equipped with an automotive-grade

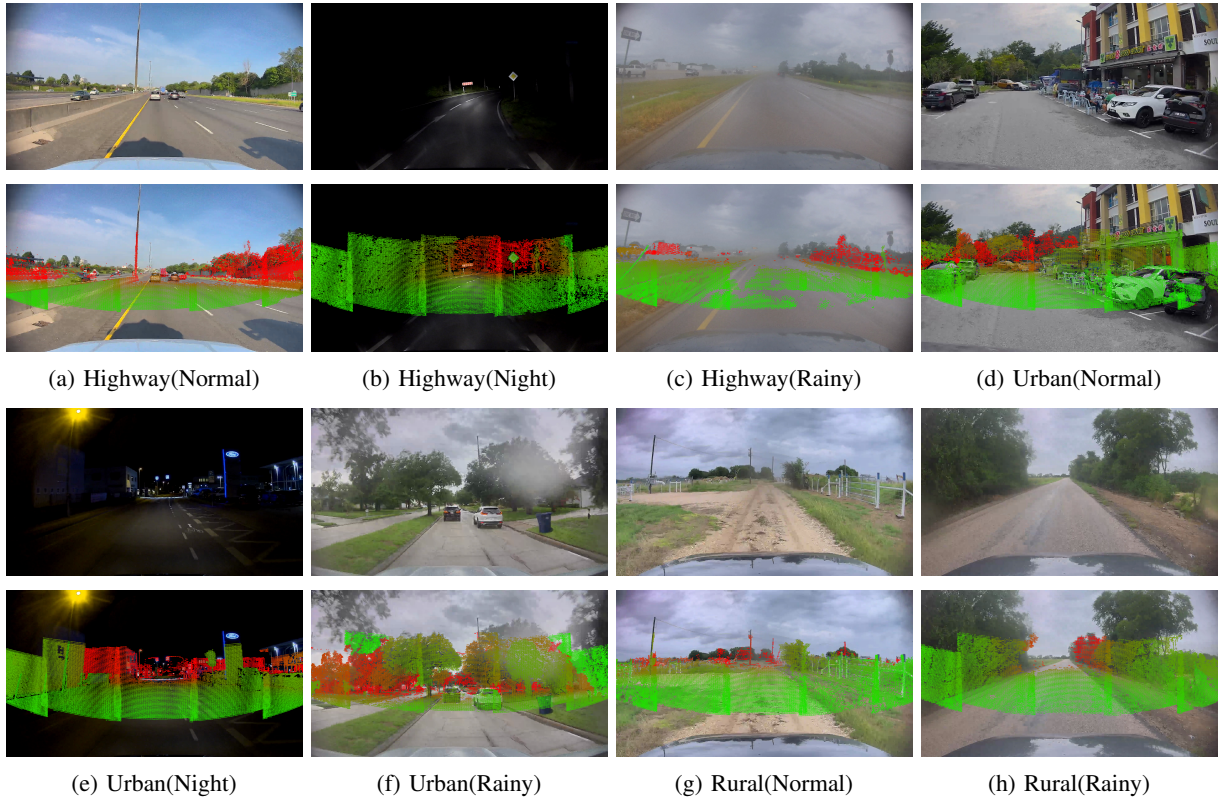


Fig. 2: **Data visualization of the ROVR dataset.** The first and third rows show RGB images, while the second and fourth rows present the corresponding depth maps projected onto the RGB images.

multi-sensor suite capable of reliable operation under diverse real-world conditions, including day/night cycles and various weather scenarios. The system has recorded over **10,000 hours** of high-quality driving data covering urban, suburban, and highway environments.

The acquisition platform integrates a 126-beam automotive-grade solid-state LiDAR, providing dense and accurate 3D point clouds with a maximum range of **200 m** and a vertical field of view of $\pm 12.5^\circ$. An automotive-grade HD RGB camera with a resolution of 1920×1080 at **30 Hz** is mounted in a forward-facing configuration and calibrated for both intrinsic and extrinsic parameters with respect to the LiDAR. The positioning system consists of a triple-frequency RTK GNSS receiver, capable of achieving centimeter-level accuracy worldwide, aided by GEODNET RTK corrections. An automotive-grade IMU with low bias instability is used for robust orientation and motion tracking. Data capture and preprocessing are performed on an embedded high-performance edge AI unit capable of 6 TOPS inference, with storage handled by a 1 TB onboard solid-state drive. All components are housed within an IP67-rated enclosure to ensure waterproof and dustproof protection.

For accurate spatial alignment, a full calibration is performed between the LiDAR, camera, GNSS, and IMU using standard multi-sensor calibration pipelines. All sensors are hardware-synchronized via GPS-disciplined clocks, achieving a temporal offset of less than **2 ms** between modalities. LiDAR

TABLE II: **Statistical overview of ROVR Open Datasets.**

Setting	Train				Test			
	Highway	Rural	Urban	Sum	Highway	Rural	Urban	Sum
Normal	114,644	6,411	42,937	163,992	5,533	600	2,080	8,213
Night	20,223	0	1,650	21,873	1,040	0	150	1,190
Rain	1,496	4,041	2,246	7,783	150	299	150	599
Sum	136,393	10,452	46,833	193,648	6,723	899	2,380	10,002

data is recorded at **5 Hz**, while camera streams operate at **5 Hz**, with each frame paired with precise vehicle pose information.

B. Data Organization and Alignment

The processed ROVR OpenDataset is released in ROS 2 bag format, with each sequence folder named as `<UTC_time>-<device_ID>-<seq_ID>-<code>`. Within each sequence, synchronized multi-modal data are stored in modality-specific subdirectories, including 1920 \times 1080 RGB images (`images/`), LiDAR point clouds in PCD format (`pointclouds/`), LiDAR-projected depth maps in single-channel PNG (`depth/`), and perception annotations (`annotation/`). Auxiliary navigation data include interpolated GNSS/INS poses (`ego_poses.json`), raw GNSS logs (`ego_poses_raw.json`), and 100 Hz IMU measurements (`imu_data.csv`). All files are timestamped at nanosecond resolution for cross-modal synchronization.

a) Multi-Sensor Calibration.: Each acquisition platform undergoes full intrinsic and extrinsic calibration prior to

TABLE III: **Performance of depth estimation models across KITTI, DDAD, nuScenes, and ROVR.** Models trained on existing datasets perform well on their own test sets but fail to generalize to ROVR.

Train	Test	lower is better ↓						higher is better ↑		
		silog	abs_rel	log10	rms	sq_rel	log_rms	δ_1	δ_2	δ_3
VA-DepthNet [41]										
KITTI [10]	KITTI [10]	6.7058	0.0472	0.0205	2.0194	0.1393	0.0739	0.9807	0.9967	0.9991
KITTI [10]	ROVR (Ours)	49.6455	0.6345	0.2977	14.9118	11.8008	0.7617	0.0904	0.2190	0.5045
DDAD [42]	DDAD [42]	11.7611	0.0940	0.0392	5.0639	0.7429	0.1319	0.9095	0.9820	0.9942
DDAD [42]	ROVR (Ours)	37.1334	0.7487	0.1831	13.1557	20.7556	0.5445	0.2309	0.6708	0.8809
nuScenes [8]	nuScenes [8]	8.2524	0.0464	0.0181	2.2801	0.3644	0.0873	0.9730	0.9837	0.9910
nuScenes [8]	ROVR (Ours)	50.7492	0.4864	0.1641	12.5946	10.4858	0.5217	0.4218	0.7016	0.8429

TABLE IV: **Cross-dataset evaluation** of three depth estimation models: training on KITTI leads to large performance drops on ROVR, while training on ROVR yields better results.

Train	Test	lower is better ↓						higher is better ↑		
		silog	abs_rel	log10	rms	sq_rel	log_rms	δ_1	δ_2	δ_3
VA-DepthNet [41]										
KITTI [10]	ROVR (Ours)	48.7576	0.5896	0.2360	13.7797	12.2677	0.6443	0.1525	0.4188	0.7517
ROVR (Ours)	ROVR (Ours)	29.3324	0.1812	0.0524	6.9541	3.9546	0.2977	0.8862	0.9366	0.9580
DCDepth [43]										
KITTI [10]	ROVR (Ours)	49.9300	0.6396	0.2895	14.9843	12.4077	0.7433	0.0653	0.2122	0.5887
ROVR (Ours)	ROVR (Ours)	27.2769	0.1943	0.0510	6.4558	4.1901	0.2786	0.8876	0.9369	0.9603
IEBins [44]										
KITTI [10]	ROVR (Ours)	48.5049	0.6078	0.2956	15.2223	10.7613	0.7563	0.0705	0.1990	0.5830
ROVR (Ours)	ROVR (Ours)	29.9729	0.2146	0.0664	7.3685	3.7523	0.3106	0.8411	0.9236	0.9520

deployment. Camera intrinsics and distortion coefficients are stored in `int.yaml`, while LiDAR-to-camera extrinsics are stored in `ext.yaml` as a Rodrigues rotation vector and translation vector, following a coordinate remapping ($x = -y, y = -z, z = x$). GNSS-IMU lever-arm offsets are estimated from synchronized motion sequences. These parameters enable precise projection of LiDAR points \mathbf{p}_l onto the camera image plane:

$$\mathbf{p}_c \sim \mathbf{K} (\mathbf{R}_{l \rightarrow c} \mathbf{p}_l + \mathbf{t}_{l \rightarrow c}), \quad (1)$$

where \mathbf{K} is the camera intrinsic matrix, and $(\mathbf{R}_{l \rightarrow c}, \mathbf{t}_{l \rightarrow c})$ are the extrinsic parameters from LiDAR to camera coordinates.

b) Data Statistics: As summarized in Table II, the ROVR OpenDataset covers a diverse set of driving environments, including highway, rural, and urban scenes under normal, night, and rainy conditions. The training split contains a total of 193,648 frames, while the test split consists of 10,002 frames. Highway driving dominates the data distribution, but the dataset also includes challenging low-light (night) and adverse-weather (rain) scenarios to promote robustness in perception models.

IV. EXPERIMENTS

We conduct experiments on the ROVR Open Dataset to establish baseline performance and to analyze the influence of different factors. The evaluation consists of (i) benchmark results on the full test split to provide a single reference point for future studies, and (ii) domain-specific results under varying illumination and scene types to illustrate different results.

A. Implementation Details

We evaluate three representative monocular depth baselines on our dataset—VA-DepthNet [41], DCDepth [43], and IEBins [44]. To ensure comparability, we reproduce the variants that adopt the Swin Transformer–Large (Swin-L) [45] backbone and initialize training solely from its pretrained weights. All images are center-cropped to 960×544 for both training and evaluation, and each model is trained for 5 epochs. Unless otherwise noted, we follow the official training configurations of each method (e.g., learning rate, weight decay). Ground-truth depth is measured in meters; during training and evaluation, depths are clipped to $[1, 80]$ meters and invalid pixels are masked. All experiments are conducted on $8 \times$ NVIDIA L20 GPUs.

B. Evaluation Metrics

We follow standard monocular depth estimation [1], [2] practice and report six error metrics where lower is better: scale-invariant log RMSE (silog), absolute relative error (abs_rel), log10 error (log10), root mean squared error (rms), squared relative error (sq_rel), and log RMSE (log_rms). We also report three accuracy metrics where higher is better: δ_1 , δ_2 , and δ_3 , representing the fraction of pixels where the prediction is within a factor of 1.25, 1.25^2 , and 1.25^3 of the ground truth.

C. Main Results

As shown in Tables III, models trained on KITTI [10], DDAD [42], or nuScenes [8] achieve strong results within their own domains, yet when transferred to ROVR, their

TABLE V: **Depth estimation performance across different conditions.** All models are trained on the unified training split and evaluated on different test sub-domains of the same dataset. The upper block reports results under varying illumination (*light conditions*), while the lower block reports results across scene types.

Domain	Method	Lower is better ↓						Higher is better ↑		
		silog	abs_rel	log10	rms	sq_rel	log_rms	δ_1	δ_2	δ_3
(a) Illumination Conditions										
Normal	VA-DepthNet [41]	29.8942	0.1833	0.0528	7.0396	4.0945	0.3035	0.8884	0.9366	0.9573
	DCDepth [43]	29.6740	0.2033	0.0551	7.0320	4.3746	0.3016	0.8756	0.9335	0.9569
	IEBins [44]	30.3786	0.2101	0.0648	7.4493	3.7839	0.3125	0.8501	0.9238	0.9509
Night	VA-DepthNet [41]	27.3737	0.1716	0.0493	6.6754	3.4274	0.2770	0.8804	0.9368	0.9617
	DCDepth [43]	27.2400	0.1785	0.0492	6.5566	3.5686	0.2755	0.8717	0.9356	0.9636
	IEBins [44]	28.3425	0.2081	0.0589	6.8354	3.7938	0.2914	0.8497	0.9263	0.9592
Rainy	VA-DepthNet [41]	25.5215	0.1709	0.0538	6.3357	3.0841	0.2597	0.8684	0.9360	0.9609
	DCDepth [43]	25.2770	0.1773	0.0549	6.2672	3.0250	0.2572	0.8597	0.9316	0.9609
	IEBins [44]	27.6484	0.2891	0.1025	7.3199	3.2361	0.3233	0.7015	0.9163	0.9532
(b) Scene Types										
Highway	VA-DepthNet [41]	26.2820	0.1476	0.0431	6.2185	3.1248	0.2661	0.9106	0.9484	0.9663
	DCDepth [43]	26.3602	0.1614	0.0450	6.2690	3.3054	0.2670	0.9015	0.9454	0.9655
	IEBins [44]	27.0938	0.1809	0.0565	6.6169	3.0320	0.2807	0.8690	0.9373	0.9613
Rural	VA-DepthNet [41]	29.1695	0.1803	0.0489	6.9052	4.1370	0.2948	0.8980	0.9420	0.9596
	DCDepth [43]	29.2167	0.2031	0.0505	6.7946	4.6425	0.2948	0.8851	0.9402	0.9611
	IEBins [44]	29.9301	0.2372	0.0731	7.4677	3.8916	0.3211	0.8352	0.9312	0.9550
Urban	VA-DepthNet [41]	38.0108	0.2763	0.0802	9.0505	6.2298	0.3883	0.8131	0.9013	0.9341
	DCDepth [43]	36.8839	0.3027	0.0821	8.8468	6.5511	0.3778	0.7930	0.8977	0.9353
	IEBins [44]	38.1213	0.3012	0.0916	9.4542	5.7344	0.3911	0.7645	0.8823	0.9246

performance drops dramatically across all metrics. Table IV reveal the saturation of existing benchmarks. SOTA methods that excel on KITTI [10] benchmarks still struggle on ROVR, showing that current approaches cannot fully adapt to its diverse and challenging scenarios. Training on ROVR yields consistent improvements across all evaluation metrics on ROVR, underscoring the critical role of scale and diversity in enabling models to generalize effectively to complex real-world scenarios. However, the absolute performance of existing methods remains unsatisfactory — for instance, the best abs_rel is still around 0.2 — indicating that current depth estimation approaches have already reached saturation on traditional datasets. This highlights the necessity of developing more practical models that can effectively learn from sparse depth ground truth and better handle the challenges presented by ROVR.

D. Ablation Study

Table V presents depth estimation performance across different illumination conditions and scene types, demonstrating the ROVR dataset’s diversity and the varying challenges posed by different environments.

Results under varying illumination conditions. The upper block of the table shows results under varying illumination conditions—Normal, Night, and Rainy. As expected, all methods perform better in normal lighting conditions, where visibility and depth prediction quality are optimal. However, the performance significantly declines in low-light conditions, especially at night, as seen in the reduction of metrics like δ_1 and δ_2 . VA-DepthNet consistently outperforms other methods in night-time settings, achieving the lowest abs_rel and rms values. The Rainy condition shows the largest performance

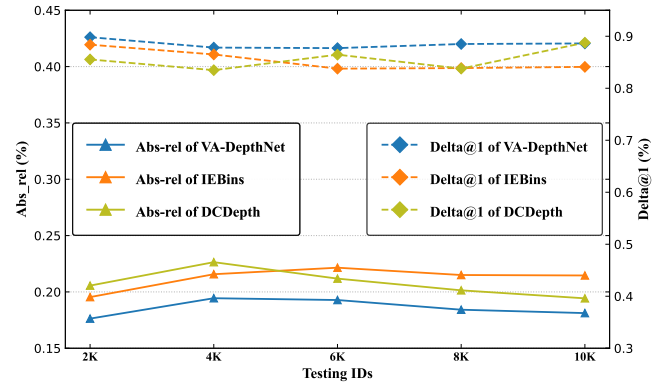


Fig. 3: **Abs_rel and δ_1 with different test identities.** The legends illustrate how performance shifts as the test data size increases from 2K to 10K.

drop, with all methods facing challenges due to degraded RGB quality and increased LiDAR sparsity. In rainy conditions, IEBins struggles the most, with substantially higher log10 and sq_rel values, indicating poor performance in handling noise and sparse data.

Results across different scene types. The lower block of the table reports results across different scene types—Highway, Rural, and Urban. Highway scenes, characterized by relatively clear and structured environments, yield the best results for all methods, with VA-DepthNet leading the pack in terms of both δ_1 and silog scores. This can be attributed to the simpler geometry and better lighting consistency typically found on highways. Conversely, Urban scenes present the greatest difficulty for depth estimation.

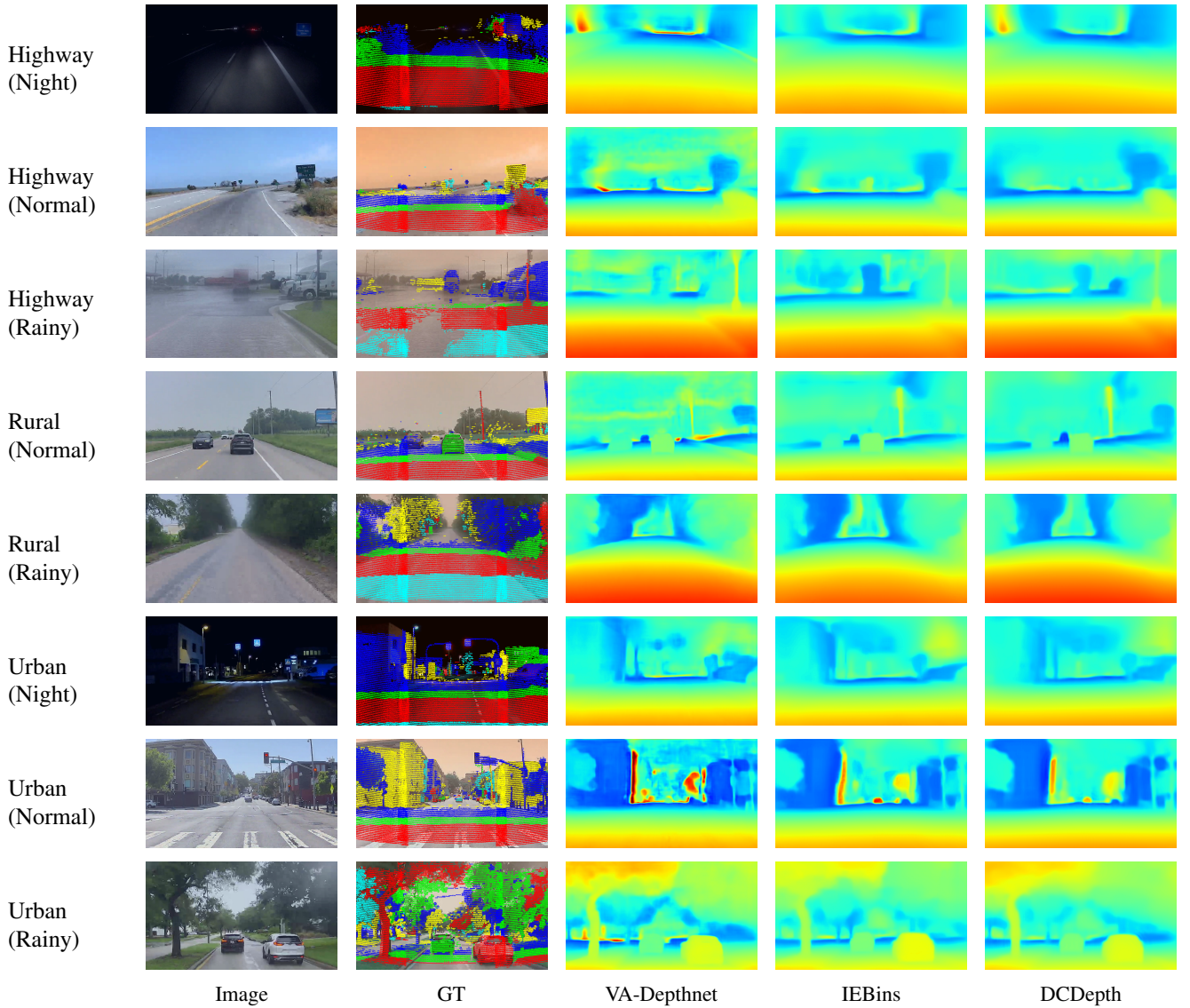


Fig. 4: **Qualitative comparisons** of depth estimation results across different scenarios (highway, rural, urban) and weather conditions (night, normal, rainy).

With complex urban layouts featuring dense clutter, frequent occlusions, and multi-scale objects, IEBins shows the largest performance gap, with noticeably higher error values across all metrics. These results highlight the challenges posed by dynamic and heterogeneous urban environments, where traditional methods struggle to maintain accuracy.

Influence of the Scale. Fig. 3 demonstrates that as the number of test identities increases from 2K to 10K, the performance curves remain relatively stable. This indicates that the ROVR dataset provides a consistent and unbiased evaluation environment, where scaling the test set does not distort the overall difficulty. Such stability highlights the dataset’s reliability as a robust benchmark for assessing depth estimation methods at large scale.

E. Qualitative Results

Fig. 4 showcases qualitative samples from the ROVR dataset across multiple scene types (highway, rural, urban)

and varying illumination and weather conditions (normal, night, rainy). Examples are drawn from different illumination conditions and scene types to match the settings in Table V. These examples highlight the dataset’s challenging nature: adverse weather and nighttime conditions significantly degrade image quality and reduce ground-truth density, while urban environments introduce dense clutter, occlusions, and multi-scale structures. Such diversity and difficulty expose clear failure modes in existing models, indicating that ROVR not only reflects real-world driving challenges but also sets a demanding benchmark for the next generation of depth estimation methods.

V. CONCLUSION

We introduced ROVR, a large-scale, diverse, and cost-efficient depth dataset designed to reflect the complexity of real-world driving. Covering varied scenes, weather, and illumination conditions, ROVR provides sparse yet statistically

sufficient ground truth, enabling robust training while imposing greater generalization challenges. Benchmarking strong KITTI SOTA models revealed substantial performance drops, underscoring the dataset’s difficulty and the limitations of existing benchmarks. By offering a challenging and extensible platform, ROVR aims to drive the development of depth estimation methods capable of handling complex, dynamic, and diverse real-world environments.

Acknowledgements. This work was supported by ROVR Labs, Inc.

REFERENCES

- [1] C. Zhao, Y. Zhang, M. Poggi, F. Tosi, X. Guo, Z. Zhu, G. Huang, Y. Tang, and S. Mattoccia, “Monovit: Self-supervised monocular depth estimation with a vision transformer,” in *International Conference on 3D Vision*, 2022.
- [2] Y. Duan, X. Guo, and Z. Zhu, “Diffusiondepth: Diffusion denoising approach for monocular depth estimation,” *ECCV*, 2024.
- [3] X. Guo, J. Lu, C. Zhang, Y. Wang, Y. Duan, T. Yang, Z. Zhu, and L. Chen, “Openstereo: A comprehensive benchmark for stereo matching and strong baseline,” *arXiv preprint arXiv:2312.00343*, 2023.
- [4] X. Guo, C. Zhang, Y. Zhang, W. Zheng, D. Nie, M. Poggi, and L. Chen, “Lightstereo: Channel boost is all you need for efficient 2d cost aggregation,” in *ICRA*, 2025.
- [5] F. Westermeier, L. Brübach, C. Wienrich, and M. E. Latoschik, “Assessing depth perception in vr and video see-through: A comparison on distance judgment, performance, and preference,” *IEEE Transactions on Visualization and Computer Graphics*, vol. 30, no. 5, pp. 2140–2150, 2024.
- [6] A. Geiger, P. Lenz, and R. Urtasun, “Are we ready for autonomous driving? the kitti vision benchmark suite,” in *CVPR*, 2012.
- [7] M. Menze and A. Geiger, “Object scene flow for autonomous vehicles,” in *CVPR*, 2015.
- [8] H. Caesar, V. Bankiti, A. H. Lang, S. Vora, V. E. Liong, Q. Xu, A. Krishnan, Y. Pan, G. Baldan, and O. Beijbom, “nuscenes: A multimodal dataset for autonomous driving,” in *CVPR*, 2020.
- [9] V. Guizilini, R. Ambrus, S. Pillai, A. Raventos, and A. Gaidon, “3d packing for self-supervised monocular depth estimation,” in *IEEE Conference on Computer Vision and Pattern Recognition (CVPR)*, 2020.
- [10] J. Uhrig, N. Schneider, L. Schneider, U. Franke, T. Brox, and A. Geiger, “Sparsity invariant cnns,” in *3DV*, 2017.
- [11] L. Yang, B. Kang, Z. Huang, Z. Zhao, X. Xu, J. Feng, and H. Zhao, “Depth anything v2,” *arXiv:2406.09414*, 2024.
- [12] L. Yang, B. Kang, Z. Huang, X. Xu, J. Feng, and H. Zhao, “Depth anything: Unleashing the power of large-scale unlabeled data,” in *CVPR*, 2024.
- [13] N. Silberman, D. Hoiem, P. Kohli, and R. Fergus, “Indoor segmentation and support inference from RGBD images,” in *ECCV*, 2012.
- [14] A. Dai, A. X. Chang, M. Savva *et al.*, “ScanNet: Richly-annotated 3d reconstructions of indoor scenes,” in *CVPR*, 2017, pp. 2432–2443.
- [15] Z. Li and N. Snavely, “MegaDepth: Learning single-view depth prediction from internet photos,” in *CVPR*, 2018, pp. 2041–2050.
- [16] J. Sturm, N. Engelhard, F. Endres, W. Burgard, and D. Cremers, “A benchmark for the evaluation of RGB-D SLAM systems,” in *IROS*, 2012, pp. 573–580.
- [17] J. McCormac, A. Handa, S. Leutenegger, and A. J. Davison, “SceneNet RGB-D: Can 5m synthetic images beat generic imagenet pre-training on indoor segmentation?” in *ICCV*, 2017, pp. 2678–2687.
- [18] M. Cordts, M. Omran, S. Ramos, T. Rehfeld, M. Enzweiler, R. Benenson, U. Franke, S. Roth, and B. Schiele, “The cityscapes dataset for semantic urban scene understanding,” in *CVPR*, 2016.
- [19] W. Maddern, G. Pascoe, C. Linegar, and P. Newman, “1 Year, 1000km: The Oxford RobotCar Dataset,” *The International Journal of Robotics Research (IJRR)*, vol. 36, no. 1, pp. 3–15, 2017. [Online]. Available: <http://dx.doi.org/10.1177/0278364916679498>
- [20] G. Yang, X. Song, C. Huang, Z. Deng, J. Shi, and B. Zhou, “Drivingstereo: A large-scale dataset for stereo matching in autonomous driving scenarios,” in *CVPR*, 2019.
- [21] P. Sun, H. Kretzschmar, X. Dotiwalla, A. Chouard, V. Patnaik, P. Tsui, J. Guo, Y. Zhou, Y. Chai, B. Caine, V. Vasudevan, W. Han, J. Ngiam, H. Zhao, A. Timofeev, S. Ettinger, M. Krivokon, A. Gao, A. Joshi, Y. Zhang, J. Shlens, Z. Chen, and D. Anguelov, “Scalability in perception for autonomous driving: Waymo open dataset,” in *Proceedings of the IEEE/CVF Conference on Computer Vision and Pattern Recognition (CVPR)*, June 2020.
- [22] I. Vasiljevic, N. Kolkin, S. Zhang, R. Luo, H. Wang, F. Z. Dai, A. F. Daniele, M. Mostajabi, S. Basart, M. R. Walter, and G. Shakhnarovich, “DIODE: A Dense Indoor and Outdoor DEpth Dataset,” *CoRR*, vol. abs/1908.00463, 2019. [Online]. Available: <http://arxiv.org/abs/1908.00463>
- [23] D. Eigen, C. Puhrsch, and R. Fergus, “Depth map prediction from a single image using a multi-scale deep network,” in *NeurIPS*, 2014.
- [24] H. Fu, M. Gong, C. Wang, K. Batmanghelich, and D. Tao, “Deep ordinal regression network for monocular depth estimation,” *Proceedings of the IEEE/CVF Conference on Computer Vision and Pattern Recognition (CVPR)*, pp. 2002–2011, 6 2018. [Online]. Available: <https://arxiv.org/abs/1806.02446v1>
- [25] I. Laina, C. Rupprecht, V. Belagiannis, F. Tombari, and N. Navab, “Deeper depth prediction with fully convolutional residual networks,” *Proceedings of the International Conference on 3D Vision (3DV)*, pp. 239–248, 6 2016. [Online]. Available: <https://arxiv.org/abs/1606.00373v2>
- [26] F. Liu, C. Shen, G. Lin, and I. Reid, “Learning depth from single monocular images using deep convolutional neural fields,” *IEEE Transactions on Pattern Analysis and Machine Intelligence (T-PAMI)*, vol. 38, pp. 2024–2039, 2 2015. [Online]. Available: <http://arxiv.org/abs/1502.07411> <http://dx.doi.org/10.1109/TPAMI.2015.2505283>
- [27] V. Patil, C. Sakaridis, A. Liniger, and L. V. Gool, “P3Depth: Monocular depth estimation with a piecewise planarity prior,” in *CVPR*, 2022.
- [28] G. Yang, H. Tang, M. Ding, N. Sebe, and E. Ricci, “Transformer-based attention networks for continuous pixel-wise prediction,” *Proceedings of the IEEE/CVF International Conference on Computer Vision (ICCV)*, pp. 16 249–16 259, 3 2021. [Online]. Available: <https://arxiv.org/abs/2103.12091v2>
- [29] S. F. Bhat, I. Alhashim, and P. Wonka, “Adabins: Depth estimation using adaptive bins,” *Proceedings of the IEEE/CVF Conference on Computer Vision and Pattern Recognition (CVPR)*, pp. 4008–4017, 11 2020. [Online]. Available: <http://arxiv.org/abs/2011.14141> <http://dx.doi.org/10.1109/CVPR46437.2021.00400>
- [30] W. Yuan, X. Gu, Z. Dai, S. Zhu, and P. Tan, “Neural window fully-connected crfs for monocular depth estimation,” in *Proceedings of the IEEE/CVF Conference on Computer Vision and Pattern Recognition (CVPR)*. IEEE, 2022, pp. 3906–3915. [Online]. Available: <https://doi.org/10.1109/CVPR52688.2022.00389>
- [31] L. Piccinelli, C. Sakaridis, and F. Yu, “iDisc: Internal discretization for monocular depth estimation,” in *Proceedings of the IEEE/CVF Conference on Computer Vision and Pattern Recognition (CVPR)*, 2023.
- [32] R. Ranftl, A. Bochkovskiy, and V. Koltun, “Vision transformers for dense prediction,” in *ICCV*, 2021.
- [33] L. Yang, B. Kang, Z. Huang, Z. Zhao, X. Xu, J. Feng, and H. Zhao, “Depth anything v2,” *arXiv preprint arXiv:2406.09414*, 2024.
- [34] S. F. Bhat, R. Birkel, D. Wofk, P. Wonka, and M. Müller, “Zoedepth: Zero-shot transfer by combining relative and metric depth,” *arXiv preprint arXiv:2302.12288*, 2023.
- [35] V. Guizilini, I. Vasiljevic, D. Chen, R. Ambrus, and A. Gaidon, “Towards zero-shot scale-aware monocular depth estimation,” in *Proceedings of the IEEE/CVF International Conference on Computer Vision (ICCV)*, 2023, pp. 9233–9243.
- [36] W. Yin, C. Zhang, H. Chen, Z. Cai, G. Yu, K. Wang, X. Chen, and C. Shen, “Metric3d: Towards zero-shot metric 3d prediction from a single image,” in *Proceedings of the IEEE/CVF International Conference on Computer Vision (ICCV)*, 2023, pp. 9043–9053.
- [37] J. M. Facil, B. Ummenhofer, H. Zhou, L. Montesano, T. Brox, and J. Civera, “Cam-convs: Camera-aware multi-scale convolutions for single-view depth,” in *Proceedings of the IEEE/CVF Conference on Computer Vision and Pattern Recognition (CVPR)*, 2019, pp. 11 826–11 835.
- [38] J. H. Lee, M. Han, D. W. Ko, and I. H. Suh, “From big to small: Multi-scale local planar guidance for monocular depth estimation,” *CoRR*, vol. abs/1907.10326, 7 2019. [Online]. Available: <http://arxiv.org/abs/1907.10326>

- [39] M. L. Antequera, P. Gargallo, M. Hofinger, S. R. Bulò, Y. Kuang, and P. Kotschieder, "Mapillary planet-scale depth dataset," in *The European Conference Computer Vision (ECCV)*. Springer International Publishing, 2020, pp. 589–604.
- [40] B. Ke, A. Obukhov, S. Huang, N. Metzger, R. C. Daudt, and K. Schindler, "Repurposing diffusion-based image generators for monocular depth estimation," in *CVPR*, 2024.
- [41] C. Liu, S. Kumar, S. Gu, R. Timofte, and L. Van Gool, "Va-depthnet: A variational approach to single image depth prediction," *arXiv preprint arXiv:2302.06556*, 2023.
- [42] V. Guizilini, R. Ambrus, S. Pillai, A. Raventos, and A. Gaidon, "3d packing for self-supervised monocular depth estimation," in *Proceedings of the IEEE/CVF Conference on Computer Vision and Pattern Recognition (CVPR)*, 2020.
- [43] K. Wang, Z. Yan, J. Fan, W. Zhu, X. Li, J. Li, and J. Yang, "Dcdepth: Progressive monocular depth estimation in discrete cosine domain," *Advances in Neural Information Processing Systems*, vol. 37, pp. 64 629–64 648, 2024.
- [44] S. Shao, Z. Pei, X. Wu, Z. Liu, W. Chen, and Z. Li, "Iebins: Iterative elastic bins for monocular depth estimation," *Advances in Neural Information Processing Systems*, vol. 36, pp. 53 025–53 037, 2023.
- [45] Z. Liu, Y. Lin, Y. Cao, H. Hu, Y. Wei, Z. Zhang, S. Lin, and B. Guo, "Swin transformer: Hierarchical vision transformer using shifted windows," in *Proceedings of the IEEE/CVF International Conference on Computer Vision (ICCV)*, 2021.